The dynamical consequences of seasonal forcing, immune boosting and demographic change in a model of disease transmission

Mathew P. Dafilis[a,b], Federico Frascoli[c], Jodie McVernon[a,b], Jane M. Heffernan[a,d,e], James M. McCaw[a,b,*]

[a] *Melbourne School of Population and Global Health, The University of Melbourne, VIC, Australia*
[b] *Murdoch Childrens Research Institute, VIC, Australia*
[c] *Department of Mathematics, Faculty of Science, Engineering and Technology, Swinburne University of Technology, VIC, Australia*
[d] *Modelling Infection and Immunity Lab, Centre for Disease Modelling, York Institute for Health Research*
[e] *Mathematics and Statistics, York University, ON, Canada*

Abstract

The impact of seasonal effects on the time course of an infectious disease can be dramatic. Seasonal fluctuations in the transmission rate for an infectious disease are known mathematically to induce cyclical behaviour and drive the onset of multistable and chaotic dynamics. These properties of forced dynamical systems have previously been used to explain observed changes in the period of outbreaks of infections such as measles, varicella (chickenpox), rubella and pertussis (whooping cough). Here, we examine in detail the dynamical properties of a seasonally forced extension of a model of infection previously used to study pertussis. The model is novel in that it includes a non-linear feedback term capturing the interaction between exposure and the duration of protection against re-infection. We show that the presence of limit cycles and multistability in the *unforced system* give rise to complex and intricate behaviour as seasonal forcing is introduced. Through a mixture of numerical simulation and bifurcation analysis, we identify and explain the origins of chaotic regions of parameter space. Furthermore, we identify regions where saddle node lines and

*Corresponding author: jamesm@unimelb.edu.au, +613 8344 9145, Level 3, 207 Bouverie St, Carlton VIC 3010, Australia

period-doubling cascades of different orbital periods overlap, suggesting that the system is particularly sensitive to small perturbations in its parameters and prone to multistable behaviour. From a public health point of view — framed through the 'demographic transition' whereby a population's birth rate drops over time (and life-expectancy commensurately increases) — we argue that even weak levels of seasonal-forcing and immune boosting may contribute to the myriad of complex and unexpected epidemiological behaviours observed for diseases such as pertussis. Our approach helps to contextualise these epidemiological observations and provides guidance on how to consider the potential impact of vaccination programs.

Keywords: infectious disease, seasonal forcing, immunity, multistability, chaos, bifurcation analysis

---

1. Introduction

The impact of seasonal effects on the time course of an infectious disease can be dramatic. Two well-known examples are the observed winter-onset of influenza in temperate climates [29], and the seasonal fluctuation in incidence of mosquito-borne diseases such as dengue [1]. While the latter is well understood as a direct consequence of the role of climatic factors in driving annual fluctuations in the mosquito population size, the underlying causes for the former are imperfectly understood. Influenza seasonality may involve a range of climatic variables such as temperature and humidity that interact with biological (e.g. virus survival) and sociological (e.g. human contact and mixing behaviour) factors [2, 29]. Many other diseases, such as measles, varicella (chickenpox), rubella and pertussis (whooping cough) also display seasonal characteristics which, importantly, have changed over the course of the 20^{th} Century [3].

From the mathematical point of view, the effects of seasonal forcing in an epidemiological context can be studied in a number of ways. The first and foremost is the bifurcation approach, through which variations in model solutions due to changes in system parameters are analyzed using bifurcation diagrams

[26]. As the intensity and frequency of seasonal forcing are varied, the appearance of forced oscillations in the population can be studied systematically. Many studies of such systems exist in the literature, see for example Bolzoni et al. [5], Kuznetsov and Piccardi [25], Kuznetsov et al. [27], Rinaldi and Muratori [31], Doveri et al. [10], Scheffer et al. [34], Rinaldi et al. [32] and Tanaka and Aihara [35]. Related examples include an analysis of seasonal forcing for a predator-prey model [36] and the study of a model for immune priming [4].

Other approaches to analysing such models include resonance theory [17] or perturbation methods [23, 24] which have been used elsewhere successfully in models relevant for epidemiology, ecology and demography [33, 18, 19, 37, 6, 20]. In the context of infectious diseases, Earn et al. [11] demonstrated that transitions from predictable to unpredictable, and potentially chaotic, behaviour for childhood diseases such as measles may arise naturally from changes in birth rates and/or vaccination schedules once seasonal fluctuations in the rate of infection were accounted for. In all these works, parameters that regulate the strength and periodicity of seasonal variations are shown to be responsible for the birth of complex phenomena of interest from both the biological and mathematical point of view, including multi-year cycles, chaotic dynamics, intermittent and catastrophic behaviors and multistable states.

In recent work, we used a combination of bifurcation analysis and numerical simulation to study the dynamics of a previously published model of pertussis infection [28] in which protection following infection is not lifelong and immunity may be 'boosted' due to continual circulation of disease [8]. Where Lavine et al. [28] focussed on the role of vaccination in inducing undamped oscillatory dynamics, we demonstrated that a declining in the birth-rate, as observed in Western populations over the past century, was capable of transitioning the system from one characterised by endemic steady-state dynamics to one in which sustained (undamped) oscillations in disease prevalence characterised the system. Our and Lavine et al. [28]'s results were derived in the absence of any seasonal fluctuations in the transmissibility of the pathogen.

In this paper we extend the model to include seasonal forcing and investi-

gate the model's behaviour using bifurcation analysis and numerical simulation. Particular attention is devoted to understanding how changes in the strength of immune boosting and the intensity of seasonal forcing elicit different behaviour, and how such behaviour varies with the assumed birth-rate for the population.

The paper is organized as follows. In Section 2 we introduce the model of transmission. A discussion of the analytic and computational techniques used for our analysis is provided in Section 3. Section 4 presents the main findings. We discuss the epidemiological consequences of our study in Section 5.

2. The SIRWS model with demography and immune boosting

Extending the classic *S*usceptible–*I*nfectious–*R*emoved mode of disease dynamics, Lavine et al. [28] introduced the 'SIRWS' model in which the population is separated into those who are susceptible to infection (S), those infected and infectious (I), those recovered, no longer infectious and immune to re-infection (R) and those whose immunity has waned sufficiently such that exposure, while not leading to productive infection, provides a 'boost' to immunity (W). Figure 1 shows the population compartments and associated flows. Assuming mass action dynamics, the corresponding equations for the model are:

$$\frac{dS}{dt} = -\beta(t)IS + 2\kappa W + \xi(1 - S) \tag{1a}$$

$$\frac{dI}{dt} = \beta(t)IS - \gamma I - \xi I \tag{1b}$$

$$\frac{dR}{dt} = \gamma I - 2\kappa R + \nu\beta(t)IW - \xi R \tag{1c}$$

$$\frac{dW}{dt} = 2\kappa R - 2\kappa W - \nu\beta(t)IW - \xi W \tag{1d}$$

where $\beta(t) = \beta_0 \left(1 + \eta \cos\left(2\pi t\right)\right)$ is the annually-forced transmission coefficient, parameterised by a baseline value β_0 and a seasonal strength η, $1/\gamma$ is the average duration of infectiousness (in the absence of death), $1/\kappa$ is the average duration of protection (in the absense of immune boosting and death), ν is the factor describing the relevant strength of immune boosting ($W \to R$) compared to infection ($S \to I$) and ξ is the birth rate for the population. We assume a

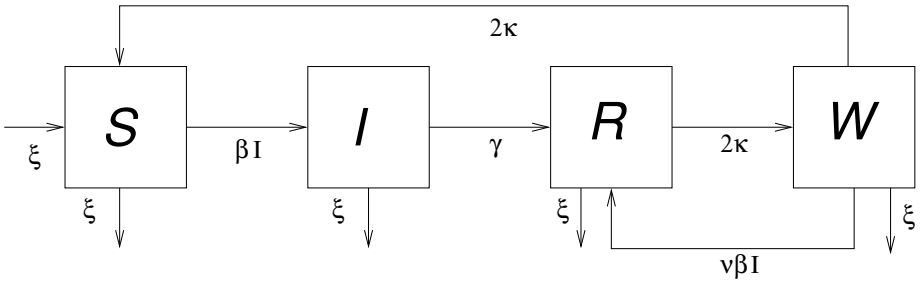

Figure 1: A schematic diagram of the SIRWS model with demography and immune boosting. In the absence of immune boosting ($\nu = 0$), the system reduces to the classic SIR(S) model, but with the return flow from R to S split into two stages. The strength of immune boosting may be less than ($\nu < 1$) or greater than ($\nu > 1$) the force of infection βI. The inclusion of this extra feedback loop in the model has fundamental consequences for the dynamical properties of the system [8].

constant population size and no infection-induced mortality, and so the death-rate is also ξ.

The key feature of the model is the second non-linear term for the transition from $W \rightarrow R$. This term is directly proportional to the force-of-infection βI and allows for the overall effective duration of immunity (the expected time to transition from R to S) to reduce as the prevalence of infection (and so disease, I) drops. Critically, the constant of proportionality, ν, may be greater than or less than one. As in earlier works [28, 8], $\nu > 1$ implies that an exposure *insufficient to initiate productive infection in a susceptible individual may nonetheless be sufficient to boost immunity*. A more detailed description of the basic mathematical properties of the model may be found in Dafilis et al. [8].

To undertake the present study on the role of seasonal-forcing (η) and its interaction with the strength of immune boosting (ν) and the population birth-rate (ξ), we must choose a set of biologically realistic parameters with which to simulate the model. Based on the aforementioned epidemiological research on pertussis [28] and our detailed study of the model's stability properties in

the absence of forcing [8], we make the following choices, noting the unit of time is set to match the natural one-year period of seasonal-forcing. The infectious duration (in the absence of births and deaths) is set to $1/\gamma = 1/17$ years (i.e. 21 days). Baseline infectiousness is set to $\beta_0 = 260$ years^{-1} yielding a basic reproduction number of ~~15.2~~$R_0 = \beta/(\gamma + \xi) \approx \beta/\gamma = 15.3$. The duration of immunity is fixed at 10 years ($\kappa = 1/10$ years^{-1}). We allow the strength of seasonal forcing (η) to lie in the range $[0, 0.5]$ and the level of immune boosting (ν) to lie in the range $[0, 20]$. We consider birth-rates between $1/50$ years^{-1} (i.e. a life-expectancy in the population of 50 years) and $1/100$ years^{-1} (i.e. a life-expectancy of 100 years).

3. Methods

In order to implement the sinusoidal forcing we used the method of Aguiar et al. [1], whereby the system of equations 1 was augmented with two additional autonomous differential equations, thereby rendering the model better suited for both numerical simulation and bifurcation analysis.

The key observable of interest is the nature of the oscillation — damped, undamped, integer or non-integer periodic (measured in years), quasiperiodic or chaotic — in infection (I) over time, as this is linked directly to disease burden. Equations 1 were numerically integrated forward in time from the initial condition of a fully susceptible population ($S(0) = 0.99, I(0) = 0.01, R(0) = 0, W(0) = 0$). The system was allowed to settle to its attractor over a period of 2000 years with the first 1000 years discarded as a transient. All subsequent calculations were performed based on the remaining 1000 year segment. Numerical integration was performed using the ODE MEX algorithm by Vanlier et al. [38].

To generate two-dimensional 'period diagrams' displaying the steady-state cyclical period of the dynamics for a chosen pair of independent model parameters, the algorithm of period detection of Taylor et al. [36] (TSW) was implemented, with two small modifications. First, we increased the detected

periods of dynamics up to 19 years (as opposed to TSW's maximum period of nine), and labelled all periods unable to be reliably detected with the label 'period 20'. These solutions may have integer periods higher than 19, non-integer periods, or be either quasiperiodic or chaotic. Second, we used a threshold of 5 percent of the mean value used in period detection as opposed to the default TSW threshold of 2.5 percent (see Taylor et al. [36] for full details). Based on extensive study of individual time-series (data not shown) this cut-off provided a more robust period detection and less false period 20 detections.

In the following, orbits are labelled n/m, where m is the periodicity of the orbit in years and n is the generation of the orbit, i.e. the number of maxima (in I) reached over the m year cycle. For example, a $1/3$ orbit has a single maxima in each three year cycle, while a $7/17$ orbit has seven peaks over a 17 year cycle.

In order to ascertain whether dynamics labelled period 20 were chaotic (as opposed to of a period higher than 19 years, of non-integer period or quasiperiodic), an implementation of the Christiansen-Rugh algorithm [7] was used to calculate the largest Lyapunov exponent (LLE). A positive LLE is an unambiguous determinant of the presence of chaotic dynamics. Chaotic dynamics were additionally confirmed using the Gottwald-Melbourne 0–1 test for chaos [12, 16, 15, 14, 13] based on S and I time series.

We examined numerically generated period diagrams in the (η, ν)-plane in tandem with bifurcation analyses, the latter performed with the software AUTO [9]. Starting from an initial, unforced solution (i.e. $\eta = 0$), the orbit was continued initially in one parameter (either η or ν), and bifurcation points were found numerically. Codimension one bifurcations were continued in both parameters η and ν, so that the loci of points that determine the region of existence for an orbit were computed. The analysis followed the standard bifurcation approach [27, 10, 34, 31, 32]. We adopt the terminology of Taylor et al. [36] and Best [4].

4. Results

Our previous work on the unforced SIRWS system has demonstrated the fundamental importance of the strength of immune boosting (ν) in determining the dynamical properties of the equations [8]. That work also demonstrated that demography, captured in a simple manner through the birth rate (ξ, or equivalently the life-expectancy ($1/\xi$)), influenced the stability properties of the model, with consequences for the interpretation of infectious disease epidemiology over the past century. Those results are summarised in figure 2, which shows regimes where point attractor, limit cycle and bistable dynamics are supported by the model, depending upon the chosen values for the birth-rate (ξ) and boosting strength (ν).

We make note of two special points in figure 2 — the limit point (`LP`) which we will henceforth denote ξ_{LP} to make clear its dependence on ξ, and the generalised Hopf (or Bautin point, `GH`), similarly denoted ξ_{GH}. For $\xi < \xi_{LP} \approx 0.01814$ there exist values of the boosting (ν) for which oscillatory dynamics exist, while for $\xi > \xi_{LP}$ the system displays damped oscillatory oscillations for all values of the boosting ν. The generalised Hopf bifurcation $\xi_{GH} \approx 0.01473$ marks the change (moving right to left) from supercritical to subcritical for the Hopf bifurcation line, giving rise to a region of bistability. We will soon see that this has dramatic implications for the forced scenario.

Noting that neither seasonal-forcing (η) nor immune-boosting (ν) is well determined biologically (and/or may vary dramatically for different diseases of interest), in what follows we consider those two parameters to be the primary independent variables for analysis, and present period diagrams and two-dimensional bifurcation diagrams on those axes. We perform our analysis for a number of fixed values for the birth-rate (ξ), illustrating the dependence of the complexity of the observed behaviour on the demographic state of the population.

Figure 3 presents a sequence of 'period diagrams', each for a fixed value of the birth rate (ξ), of the numerically detected steady-state periods in the

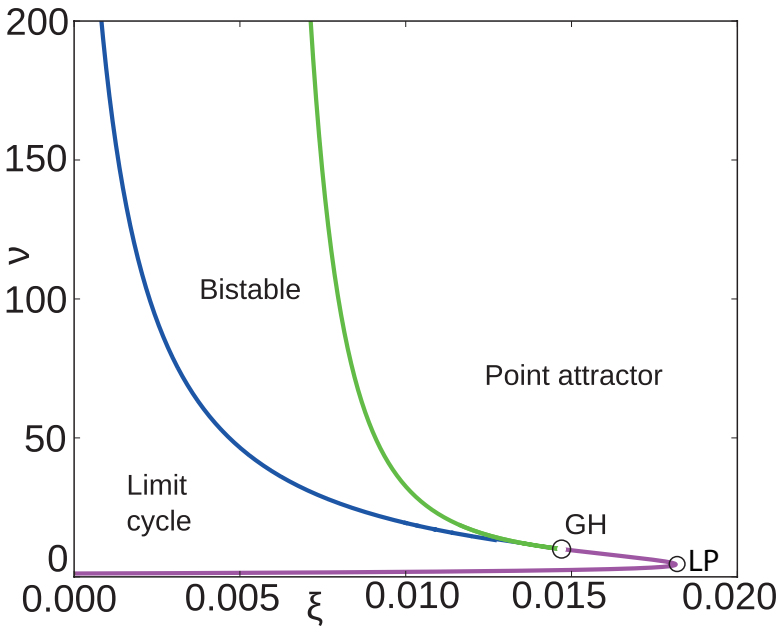

Figure 2: Stability properties of the unforced SIRWS system. A two parameter bifurcation diagram in the (ξ, ν)-plane. Lines demarcate the different regions in parameter space. The Hopf bifurcation is subcritical for $\xi < \xi_{GH}$ and supercritical otherwise, allowing for bistable behaviour for $\xi < \xi_{GH}$. The value of ξ at the kink is given by $\xi_{LP} \approx 0.01814$, and at the `GH` by $\xi_{GP} \approx 0.01473$. [Reproduced from [8]]

(η, ν)-plane. Colours represent integer periods between 1 and 19 years, and one further colour (cream) represents cycles of either period greater than 19 years, or non-integer periodic, quasiperiodic or chaotic dynamics. There is a clear evolution of the period diagrams as a function of ξ. Notable is the gradual enlargement of the period 20 regions for small η indicating the potential for chaotic dynamics to appear under conditions of weak seasonal forcing as the birth-rate decreases (life-expectancy increases) and the growth of the period-3 region encompassing more and more of the plane for moderate and larger values of η. With this overview, we now consider three representative values for the birth-rate ($\xi = 1/50$ years^{-1}, $\xi = 1/75$ years^{-1} and $\xi = 1/100$ years^{-1}) in detail.

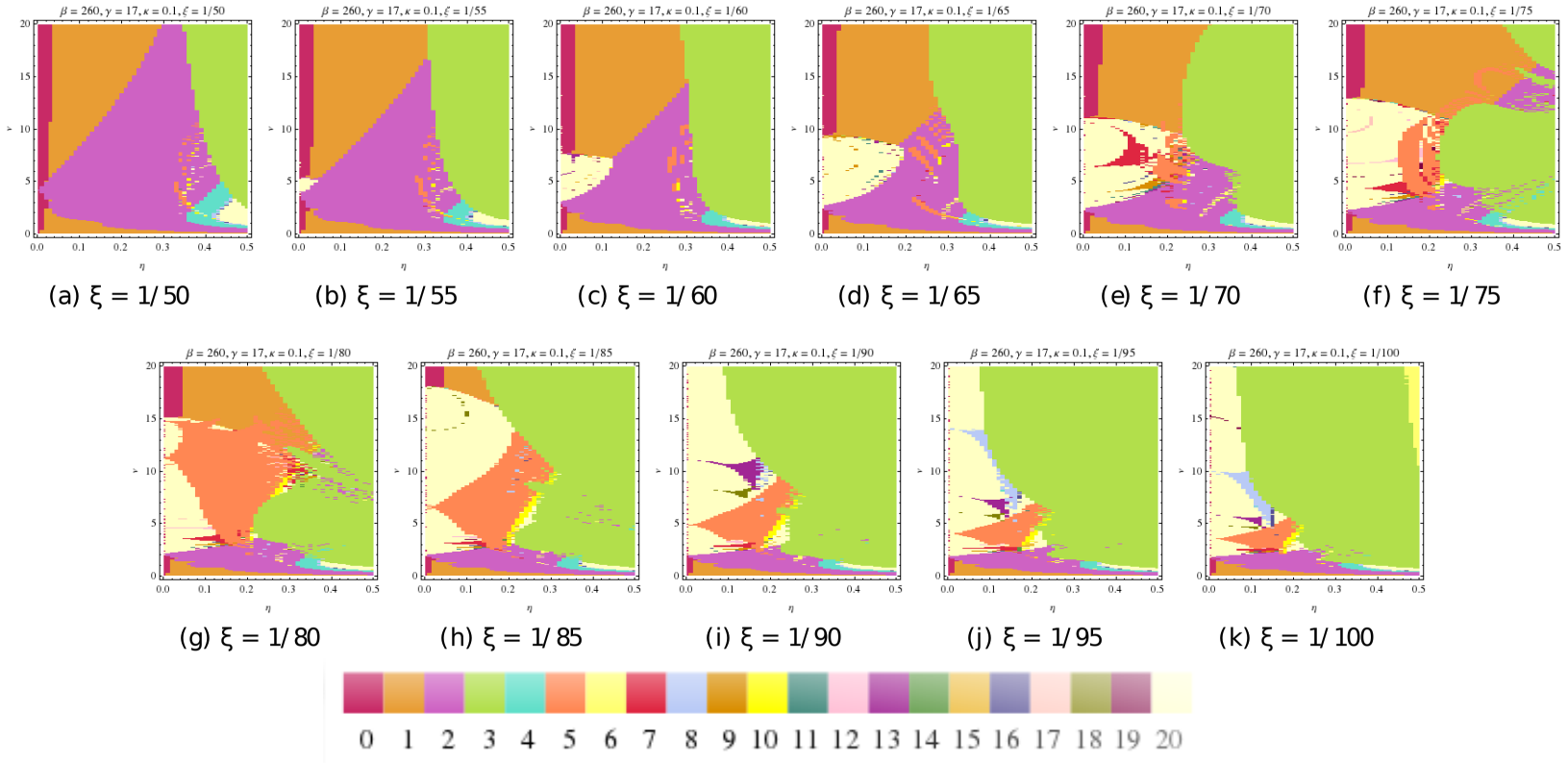

Figure 3: Period diagrams in the (η, ν)-plane for birth rates in five year intervals from (a) $\xi = 1/50$ through to (k) $\xi = 1/100$. Different colours represent different stable period orbits, labelled by their integer (measured in years) period in the colour bar. The variation in the period of oscillation of I (in years, as per legend) is shown as a function of the boosting ν (on the ordinate) and the amplitude of the seasonal forcing η (on the abscissa).

4.1. Seasonal forcing gives rise to sustained oscillations, period doublings and chaos: dynamics at a high birth-and-death rate ($\xi = 1/50 > \xi_{LP}$)

Figure 2 shows that a high birth-rate of $\xi = 0.02$, corresponding to a life-expectancy of 50 years, lies to the right of ξ_{LP}. As such, for any value of ν, the unforced model dynamics is characterized by a point attractor, i.e. the system always reaches an equilibrium at a finite time through a damped oscillatory trajectory [8]. Figure 4(a) presents the period diagram of the numerically detected steady-state periods in the (η, ν)-plane ($\xi = 1/50$ fixed).

Due to the separation between $\xi = 1/50$ and $\xi = \xi_{LP}$, weak forcing (small η) is unable to give birth to an oscillatory response and the ~~dynamics remains characterised as per~~ steady-state dynamics exhibit small amplitude annual fluctuations, in phase with the forcing, about the unforced dynamics~~by an~~ ' equilibrium trajectory (red) for all considered values of the boosting strength (ν). As the forcing increases a regime of oscillations of period 2 arises for $\nu \approx 4$. These cycles first appear for this intermediate value of ν due to the proximity to ξ_{LP} (i.e. close to the kink in figure 2). At values close to ξ_{LP}, *unforced* trajectories have long oscillatory transients before reaching the equilibrium (i.e. they are very weakly damped), and so are particularly responsive to seasonal forcing. In consequence, the damped unforced trajectory nearby the limit point (ξ_{LP}) can be entrained into a stable limit cycle. This particular response represents a so-called 1/2 orbit in the variable $I(t)$: as a result of the phase-locking with the external driving force [30], the model displays a two year cycle characterized by one maximum. This area of parameter space is particularly interesting because, as the birth-rate (ξ) decreases, it corresponds to the zone of limit cycles in the unforced model. For larger or smaller values of ν, the strength of seasonal forcing must be somewhat larger to entrain the trajectory, explaining the shape of the 1/2 orbit region (magenta) in figure 4(a). Other key features in figure 4(a) include the presence of 1/1 orbits (orange) at intermediate values for forcing and low and high values for the boosting. Interestingly, 1/2 orbits displace the 1/1 orbits as seasonality increases. For $\nu \lessapprox 10$, values for forcing beyond $\eta \approx 0.33$ give rise to new orbits with longer periods. Most obvious are period 5

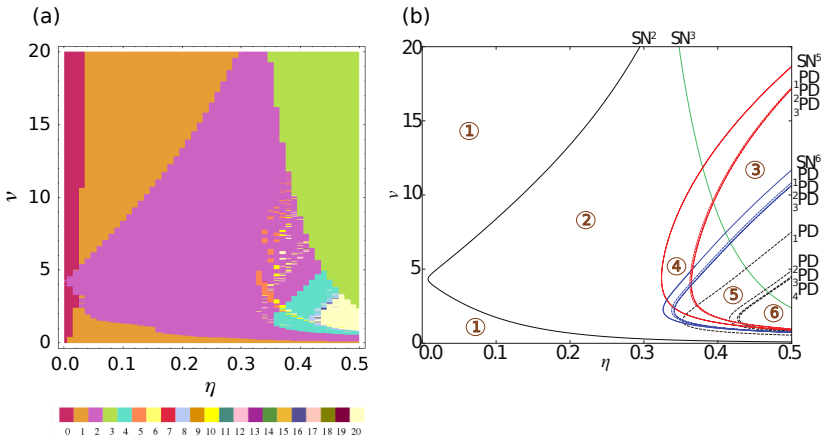

Figure 4: Period and bifurcation diagrams for $\xi = 1/50$. (a) The period diagram in the (η, ν)-plane. Different colours represent different stable periodic orbits. For very weak seasonal forcing ($\eta \approx 0$) the system ~~displays damped periodic behaviour~~ remains characterised by the unforced system's point attractor dynamics (see figure 2). It exhibits small amplitude in-phase annual fluctuations about the unforced system's equilibrium trajectory (red) for all values of the boosting (ν)~~as per the unforced system (see figure 2)~~. For larger values of the forcing ~~we~~ the trajectories may be entrained into stable limit cycles. We observe a number of different periods as discussed in detail in the main text. (b) The corresponding two parameter diagram for bifurcation points of forced orbits in the (η, ν)-plane. Saddle node lines ($\mathtt{SN}^m$, solid) denote the boundary for areas in which period m orbits may be sustained. Period doubling lines (${}_n\mathtt{PD}^m$, dashed) indicate where n^{th}-generation orbits of the period-m cascade are present. The regions labelled ① through ⑥ are used to guide the discussion in the main text.

and period 6 orbits interspersed in the sea of 1/2 orbits. At higher values for the boosting ($\nu \gtrapprox 10$), a regime of 1/3 oscillations (green) emerges. As η increases further, period 2 orbits give way to a period-doubling cascade of higher order orbits (period 4 (cyan), 8 (light blue) and 16 (mauve)), eventuating in an area beyond $\eta \approx 0.43$ labelled as period 20 and confirmed (using the aforementioned LLE and 0–1 test methods) to sustain chaotic dynamics.

To understand why these dynamical phenomena are present, a bifurcation analysis which complements the period diagram is presented in figure 4(b). Two types of lines are presented: Saddle node lines ($\mathtt{SN}^m$, solid) mark the boundary for areas in which period m orbits may be sustained. Period doubling lines (${}_n\mathtt{PD}^m$, dashed) indicate where n^{th}-generation orbits of the period-m cascade may arise.

A visual inspection of the diagram (figure 4(b)) confirms our description of the numerical period diagram (figure 4(a)). To the left of line $\mathtt{SN}^2$ (marked as region 1 in the diagram) only period 1 orbits are sustainable. Note that we don't resolve the bifurcation line indicating the onset of sustained oscillations (as opposed to damped oscillatory behaviour). To the right of $\mathtt{SN}^2$ period two oscillations are sustained (region 2 in the diagram). Similarly, to the right of $\mathtt{SN}^3$, $\mathtt{SN}^5$ and $\mathtt{SN}^6$ the system supports period three (1/3), five (2/5) and six (3/6) oscillations respectively. Immediately obvious is that these regions overlap, suggesting that more than one type of orbit may occur for a given combination of parameters η and ν, depending on the initial condition at $t = 0$ for equations 1. In region 3 in the diagram we find no numerical evidence for these overlapping orbits, while in region 4 we detect the presence of small regions in which period 5 and period 6 orbits arise from our chosen initial condition. A detailed analysis of which orbits dominate and the detailed structure of the basins of attraction in these overlapping regions is the topic of a companion paper (to appear).

As forcing increases, sustained orbits have the tendency to undergo period doubling bifurcations, whose loci are indicated by the dashed lines in figure 4(b). Three ($m = 5$ or 6) or four ($m = 2$) generations of the period doubling cascade

for cycles of length m are shown. As an example, consider a 1/2 orbit in region 2. As η is increased and we cross the ${}_1\mathtt{PD}^2$ line the cycle transitions to a 2/4 orbit (i.e. two peaks are displayed in a four year repeating cycling, region 5 in the diagram). Beyond ${}_2\mathtt{PD}^2$ a 4/8 cycle is born, followed by an 8/16 cycle and so on as η is increased and further lines of period doubling are crossed, eventually resulting in chaos (region 6 in the diagram). Detailed inspection of the numerical and bifurcation diagrams reveals that a rich array of cycles are supported, including 4/10 (arising from the doubling of 2/5) and 6/12 (arising from the doubling of 3/6) orbits. Note that due to the limitations in the numerical resolution of figure 4(a) and the fixed initital condition, not every orbit present in the model is depicted in the figure. In particular, due to the chosen initial conditions we have only detected the period-doubling route to chaos for the 1/2 orbit cascade. While further analysis confirms their existence (not shown), we do not detect the period-doubling route to chaotic seas for the period 5 and period 6 orbits.

Finally, to complete our analysis of the dynamical properties of the system for a birth-rate of $\xi = 1/50$, in figure 5 we present representative time-series plots chosen from regions of the period diagram (figure 4).

4.2. The relationship between forced orbits and the period of oscillations in the unforced system: Arnold tongues at a moderate birth-and-death rate ($\xi = 1/75 \approx \xi_{GH}$)

Inspection of figure 2 shows that a birth-rate of $\xi = 1/75 = 0.01\overline{3}$ lies just to the left of the GH ($\xi_{GH} \approx 0.01473$) in a region where both limit cycle, bistable and point attractor dynamics are supported by the unforced system. As a consequence, we may expect the interplay between this bifurcation point and the seasonal forcing to give rise to qualitatively more complicated dynamics in the (η, ν)-plane than for $\xi = 1/50$. The period diagram for the system with $\xi = 1/75$ is shown in figure 6 and indeed when compared to figure 4(a) we see a far more elaborate dynamics. Numerical evidence for multistability, despite our use of a fixed initial condition, is strong. Large regions of the (η, ν)-plane pick

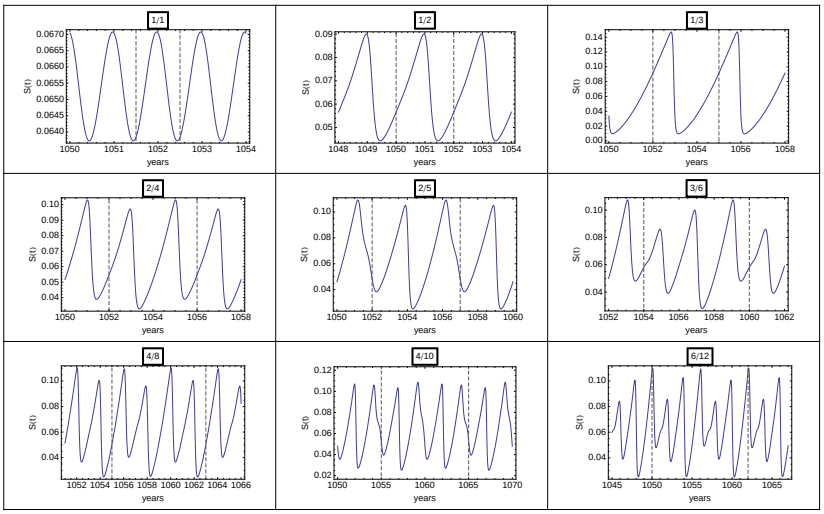

Figure 5: Time series for $\xi = 1/50$. Examples of all the cycles occurring for the case $\xi = 1/50$ that have been found in the period diagram (figure 4). For a n/m cycle, vertical lines delimit the period m of each orbit, whereas the number of maxima over the period are indicated by n.

up intermingled and scattered higher order periods, and the boundaries between dominant periods (period 1 (orange), period 2 (magenta), period 3 (green) and period 5 (apricot)) are no longer sharply defined.

Also clearly visible are narrow regions in the (η, ν)-plane for which high orbital periods extend from finite η back towards the $\eta = 0$ unforced boundary. Both individual paths (e.g. the period 7 red spike converging towards $\nu \approx 4$) and semi-circular paths (e.g. the period 17 light pink path converging to both $\nu \approx 9.5$ and $\nu \approx 12$) are observed. Known as 'Arnold tongues', these features are typical of non-linear forced systems [30, 26, 17, 23] for which the unforced dynamics support limit cycles. The complex morphology that we have numerically resolved is sufficiently high so as to allow for an examination of their organisation. As described by Taylor et al. [36], for a system subjected to an external forcing with period of one (year), an n/m orbit in the *forced-system* will converge towards an orbit with a period of m/n years as the forcing is re-

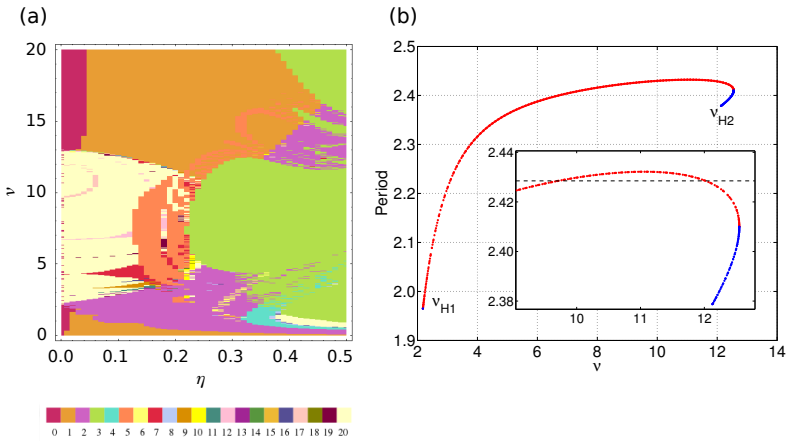

Figure 6: (a) The period diagram in the (η, ν)-plane for $\xi = 1/75$. As per figure 4(a), different colours represent different stable periodic orbits. While some features visible from the higher birth-rate scenario remain (e.g. the large pools of period 1 (orange), period 2 (magenta) and period 3 (green) attractors), the space is significantly more complex. In particular, high period regions known as Arnold tonogues extend all the way to the $\eta \to 0_+$ boundary (see main text for details). (b) The dependence of the period of oscillations on the boosting strength (ν) for the *unforced system* ($\eta = 0$). Blue points represent unstable orbits, red points stable orbits. The inset shows a magnification of the area relevant to the discussion of the horse-shoe period 17 Arnold tongue in the main text.

duced towards zero (i.e. $\eta \to 0$). For each tongue that is numerically resolved in figure 6 (others are missed due to the resolution of our numerical computations), we may compare its forced orbit to the unforced period as a function of the boosting (ν) in figure 6(b). We discuss two exemplars of the observed behaviour. The aforementioned 3/7 orbit (red) meets the $\eta = 0$ boundary at $\nu \approx 4.57$. Reading off the corresponding period from figure 6(b) yields a period of 2.35 years, very close to the expected value of $7/3 = 2.\overline{3}$. Also strongly resolved in the numerical simulations is the 7/17 orbit (light pink) which forms a tight 'horse shoe' in the sea of period 20 on the left of figure 6. For sake of argument we work in the opposite direction to our first example: the expected period for the unforced system is $17/7 \approx 2.43$ years. Inspection of the inset on figure 6(b) shows that a period of 2.43 years can be sustained by two values of the boosting, $\nu \approx 9.77$ and $\nu \approx 12.03$ and indeed we observe that the 7/17 orbit (light pink) intersects the $\eta = 0$ axis at these values for ν. In general, higher values of boosting correspond to a higher period of oscillation for the limit cycles (figure 6(b)) and so the higher the value of ν at which the tip originates, the higher is the ratio m/n. For boosting weak enough or strong enough to result in point attractor dynamics for the unforced system, the forced system's behaviour is simpler and described in similar terms to that previously discussed for a birth-rate of $\xi = 1/50$.

4.3. A return to simplicity? Arnold tongues, period doubling and chaos at low birth rates ($\xi = 1/100 < \xi_{GH}$)

A birth-rate of $\xi = 1/100$ lies well to the left of the `GH` point in figure 2 and for the range of boosting strengths considered here ($0 < \nu < 20$) the unforced system is characterised almost exclusively by limit cycle dynamics. Therefore, we expect the forced dynamics to show fewer signs of multistability and an expanded region in which Arnold tongues are observed when compared to the moderate birth-rate scenario ($\xi = 1/75$). Figure 7(a) shows the period diagram for the system, confirming these expectations.

Focusing on the Arnold tongues, figure 7(b) shows three representative sad-

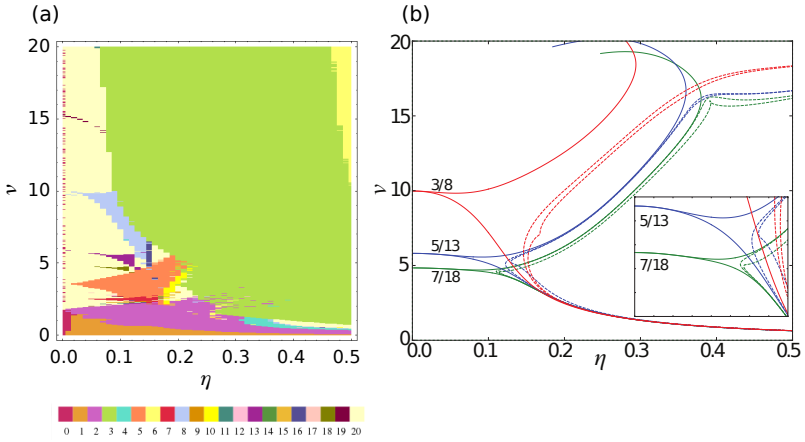

Figure 7: Period and bifurcation diagrams for $\xi = 1/100$. (a) The period diagram. As per figure 4(a), different colours represent different stable periodic orbits. The numerical signs of multistability visible in the equivalent plot for $\xi = 1/75$ (figure 6) have largely subsided. The dynamics is dominated by regions of period 1 (orange, low values of ν), period 2 (magenta) and period 3 (green) dynamics. Arnold tongues extend to the $\eta = 0$ boundary for boosting strengths up to (and beyond) the maximum sampled value ($\nu = 20$). Numerous regions of higher period orbits are also resolved. (b) The corresponding two parameter diagram for a selection of bifurcation points of forced orbits in the (η, ν)-plane, with a focus on the Arnold tongues. Saddle node lines ($\mathtt{SN}^m$, solid) denote the boundary for areas in which period m orbits may be sustained. Period doubling lines ($_n\mathtt{PD}^m$, dashed) indicate where n^{th}-generation orbits of the period-m cascade are present. Three Arnold tongues are followed from finite η back to the boundary: period 8 (red), period 13 (blue) and period 18 (green). A period doubling cascade takes place for each tongue, resulting in observable chaotic regions (clearly visible in the numerical period diagrams (a)).

dle node lines ($\mathtt{SN}^8$, $\mathtt{SN}^{13}$ and $\mathtt{SN}^{18}$, solid) extending to the $\eta = 0$ boundary and their associated period doubling lines (${}_n\mathtt{PD}^m$, dashed). Each tongue is also visible in the numerical period diagram, although the period 13 and 18 orbits (purple and olive respectively) are not fully resolved. The large period 5 tongue (apricot) is not shown in the bifurcation diagram to avoid clutter. As described in detail for the $\xi = 1/75$ scenario, the ratio m/n (i.e. the orbital period divided by the generation) corresponds to the natural period of oscillation for the unforced system for the corresponding value of the boosting (ν).

Also revealed in the period diagram (figure 7(a)) are five distinct areas (ignoring the large pool on the left) marked as period 20 (i.e. areas that *may* support chaotic dynamics). In the lower right corner we find the previously characterised (for $\xi = 1/50$) period 2 cascade resulting in a chaotic-pool for strong seasonal forcing. The other four areas occur for much lower seasonal forcing values and lie immediately to the right of the Arnold tongues just described. These pools are centered around $(\eta, \nu) \approx (0.17, 5.5)$, $(0.13, 5.0)$, $(0.12, 4.5)$ and $(0.21, 3.0)$ for the period 8, 13, 18 and 5 orbits respectively. For the period 8 and period 5 orbits we also numerically resolve the first period doubling (period 16 and period 10) region in the cascades. Note that it is numerically difficult to track down the period doubling cascades for very high period orbits and so other tongues observed in the period diagram may or may not result in chaotic regions. The LLE in these five regions is positive confirming the presence of chaotic dynamics (not shown).

5. Discussion

Our analysis has revealed the critical role that seasonal forcing, immune boosting and the birth-rate each play in determining the long-term nature of disease dynamics in the SIRWS system. We have shown how the presence of limit cycles and multistability in the *unforced system* give rise to complex and intricate behaviour as seasonal forcing is introduced. Through a mixture of numerical and analytic analysis, we have identified and explained the origins

of chaotic regions of parameter space. Furthermore, we have identified regions where saddle node lines and period-doubling cascades of different orbital periods overlap, suggesting that the observed behaviour of the SIRWS system is particularly responsive to small perturbations in its parameters.

Our results are best framed by considering the 'demographic transition' whereby a population transitions from a high birth-and-death rate to a low birth-and-death rate. As we have previously examined [8], this change in birth-rate shifts the system from beyond a point of limit cycles (where only point attractor dynamics are supported), through an intermediate region in the neighbourhood of a generalised Hopf bifurcation, and eventually to a region dominated by limit-cycle dynamics. The addition of seasonal forcing has the ability to entrain previously damped cycles onto limit-cycle attractors (figure 4) and lock periodic oscillations from the region of limit-cycles onto orbits of period m with generation number n (figure 6). Period doubling cascades, stemming from these Arnold tongues, result in chaotic dynamics for biologically plausible values of the forcing (figure 7). Noting the presence of a term proportional to $-\xi$ in each of the equations 1 (corresponding to removal due to death), we suggest that the decreased birth rate results in weaker damping of trajectories, allowing the chaotic dynamics to emerge.

From a public health point of view, the presence of large lakes of periodic behaviour, whose structure changes as the birth-rate (ξ) in the model is changed, may help to better contextualise observed changes in the epidemiological characteristics of diseases such as pertussis over the past century. While the introduction of childhood vaccination programs, beginning in the mid 20^{th} century, has undoubtedly influenced the characteristic dynamics of these infections, we have shown that minor changes in biological (e.g. ν) and/or environmental (e.g. η) factors may also contribute in a dramatic way to new and unexpected dynamics. In particular, in the high birth-rate scenario ($\xi = 1/50$) we observed that *weak* seasonal forcing, while certainly influencing the stable dynamics and potentially inducing limit-cycle behaviour, did not result in period-doublings or regions of chaos. In contrast, for lower and more realistic birth-rates ($\xi = 1/75$

and $\xi = 1/100$), weak seasonal forcing was capable of inducing substantially varied, and intricate dynamics. These results suggest that at least some of the observed changes in disease epidemiology (e.g. [11, 28, 3] and references therein) over the past century may well be due to the interaction between birth-rate and seasonality.

Two elements of the analysis deserve further attention. First and foremost is that we have not considered the effects of vaccination in our model. Both Earn et al. [11] and Lavine et al. [28] included vaccination in their models of disease transmission and showed that it too may be responsible for the induction of more complex dynamical behaviour. Both studies modelled vaccination as a 100% effective sterilising vaccine provided at birth, transferring a proportion of the births away from the susceptible (S) class and into the removed (R) class. However, the biological action of vaccines, particularly for infections such as pertussis, may be far more complicated. Rather than completely block susceptibility, they may act to modify susceptibility, infectiousness and/or the experience of disease. Furthermore, the duration of protection (against any one of those three factors) afforded by a vaccine may differ from that delivered by natural infection. None of these additional complications have been considered in the SIRWS system and all may well be expected to induce complex dynamical behaviour. Indeed, in a study by Heffernan and Keeling where a within-host model of measles capturing these more nuanced actions of immunity and vaccination was integrated into a population-level analysis [22, 21] (without seasonal forcing), large scale sustained oscillations were shown to exist. This reinforces the importance of considering such immune system and vaccination characteristics in the SIRWS system, particularly if an approach to analysis such as that taken here were to be used for a detailed study of a particular disease system.

The second point that we have not investigated in detail is the sensitivity to initial conditions. Our analysis used a fixed initial condition of a fully susceptible population. Bifurcation analysis for the unforced system (figure 2 and [8]) and the numerical studies performed here clearly indicate that alternative dynamical regimes overlap in parameter space. We may expect the basins of

attraction for these regimes to have a similarly complex morphology. In other work (to appear) we have examined the multistable properties of the seasonally-forced SIRWS system in detail, confirming the co-existence of period and chaotic attractors and the presence of dynamical crises as fundamental parameters of the model are varied. Developing a holistic overview of the dynamical structures supported by the SIRWS system, and the implications of these observations for the interpretation of epidemiological data and public health control policies for infections such as pertussis remains an open question.

Acknowledgements

JM is supported by a National Health and Medical Research Council (Australia) Career Development Fellowship. JMM is supported by an Australian Research Council Future Fellowship. MPD and FF performed the numerical analyses and drafted the first version of the manuscript. JM contributed to the public health evaluation of the findings and contextualisation of the research in terms of the existing public health literature. JH contributed to the interpretation of model findings and contextualisation of the research in terms of the existing mathematical literature. JMM formulated the scientific problem, oversaw the research, evaluated the findings and wrote the final version of the manuscript. The authors declare no competing financial interests.

References

[1] Aguiar, M., Ballesteros, S., Kooi, B.W., Stollenwerk, N.: The role of seasonality and import in a minimalistic multi-strain dengue model capturing differences between primary and secondary infections: Complex dynamics and its implications for data analysis. J. Theor. Biol. **289**, 181 – 196 (2011). DOI http://dx.doi.org/10.1016/j.jtbi.2011.08.043. URL `http://www.sciencedirect.com/science/article/pii/S0022519311004462`

[2] Altizer, S., Dobson, A., Hosseini, P., Hudson, P., Pascual, M., Rohani, P.: Seasonality and the dynamics of infectious diseases. Ecol Lett **9**(4), 467–

484 (2006). DOI 10.1111/j.1461-0248.2005.00879.x. URL http://dx.doi.org/10.1111/j.1461-0248.2005.00879.x

[3] Bauch, C.T., Earn, D.J.D.: Transients and attractors in epidemics. Proc Biol Sci **270**(1524), 1573–1578 (2003). DOI 10.1098/rspb.2003.2410. URL http://dx.doi.org/10.1098/rspb.2003.2410

[4] Best, A.: The effects of seasonal forcing on invertebrate-disease interactions with immune priming. B Math Biol **75**(11), 2241–2256 (2013). DOI 10.1007/s11538-013-9889-3. URL http://dx.doi.org/10.1007/s11538-013-9889-3

[5] Bolzoni, L., Dobson, A., Gatto, M., De Leo, G.: Allometric scaling and seasonality in the epidemics of wildlife diseases. Am. Nat. **172**(6), 818–828 (2008)

[6] Choisy, M., Gugan, J.F., Rohani, P.: Dynamics of infectious diseases and pulse vaccination: Teasing apart the embedded resonance effects. Physica D **223**(1), 26–35 (2006)

[7] Christiansen, F., Rugh, H.H.: Computing lyapunov spectra with continuous Gram - Schmidt orthonormalization. Nonlinearity **10**(5), 1063– (1997). URL http://stacks.iop.org/0951-7715/10/i=5/a=004

[8] Dafilis, M.P., Frascoli, F., Wood, J.G., McCaw, J.M.: The influence of increasing life expectancy on the dynamics of SIRS systems with immune boosting. ANZIAM J **54**, 50–63 (2012). DOI 10.1017/S1446181113000023. URL http://journals.cambridge.org/article_S1446181113000023

[9] Doedel, E.: AUTO: A program for the automatic bifurcation analysis of autonomous systems. Cong Num **30**, 265–284 (1981)

[10] Doveri, F., Scheffer, M., Rinaldi, S., Muratori, S., Kuznetsov, Y.A.: Seasonality and chaos in a plankton fish model. Theor. Popul. Biol. **43**(2), 159–183 (1993)

[11] Earn, D.J., Rohani, P., Bolker, B.M., Grenfell, B.T.: A simple model for complex dynamical transitions in epidemics. Science **287**(5453), 667–670 (2000). URL http://www.ncbi.nlm.nih.gov/pubmed/10650003

[12] Falconer, I., Gottwald, G., Melbourne, I., Wormnes, K.: Application of the 0-1 test for chaos to experimental data. SIAM J. Appl. Dyn. Syst. **6**(2), 395–402 (2007). URL http://dx.doi.org/10.1137/060672571

[13] Gottwald, G.A., Melbourne, I.: A new test for chaos in deterministic systems. Proc. R. Soc. Lond. Ser. A Math. Phys. Eng. Sci. **460**(2042), 603–611 (2004). DOI 10.1098/rspa.2003.1183. URL http://dx.doi.org/10.1098/rspa.2003.1183

[14] Gottwald, G.A., Melbourne, I.: Testing for chaos in deterministic systems with noise. Physica D **212**(1-2), 100–110 (2005). DOI 10.1016/j.physd.2005.09.011. URL http://dx.doi.org/10.1016/j.physd.2005.09.011

[15] Gottwald, G.A., Melbourne, I.: On the implementation of the 0-1 test for chaos. SIAM J. Appl. Dyn. Syst. **8**(1), 129–145 (2009). DOI 10.1137/080718851. URL http://dx.doi.org/10.1137/080718851

[16] Gottwald, G.A., Melbourne, I.: On the validity of the 0-1 test for chaos. Nonlinearity **22**(6), 1367–1382 (2009). DOI 10.1088/0951-7715/22/6/006. URL http://dx.doi.org/10.1088/0951-7715/22/6/006

[17] Greenman, J., Kamo, M., Boots, M.: External forcing of ecological and epidemiological systems: A resonance approach. Physica D **190**(1-2), 136–151 (2004)

[18] Greenman, J., Norman, R.: Environmental forcing, invasion and control of ecological and epidemiological systems. J. Theor. Biol. **247**(3), 492–506 (2007)

[19] Greenman, J., Pasour, V.: Phase control of resonant systems: Interference, chaos and high periodicity. J. Theor. Biol. **278**(1), 74–86 (2011)

[20] He, D., Earn, D.: Epidemiological effects of seasonal oscillations in birth rates. Theor. Popul. Biol. **72**(2), 274–291 (2007)

[21] Heffernan, J.M., Keeling, M.J.: An in-host model of acute infection: measles as a case study. Theor. Popul. Biol. **73**(1), 134–147 (2008). DOI 10.1016/j.tpb.2007.10.003. URL `http://dx.doi.org/10.1016/j.tpb.2007.10.003`

[22] Heffernan, J.M., Keeling, M.J.: Implications of vaccination and waning immunity. Proc Biol Sci **276**(1664), 2071–2080 (2009). DOI 10.1098/rspb.2009.0057. URL `http://dx.doi.org/10.1098/rspb.2009.0057`

[23] King, A., Schaffer, W.: The rainbow bridge: Hamiltonian limits and resonance in predator-prey dynamics. J. Math. Biol. **39**(5), 439–469 (1999)

[24] King, A., Schaffer, W.: The geometry of a population cycle: A mechanistic model of snowshoe hare demography. Ecology **82**(3), 814–830 (2001)

[25] Kuznetsov, Y., Piccardi, C.: Bifurcation analysis pf periodic seir and sir epidemic models. J. Math. Biol. **32**(2), 109–121 (1994)

[26] Kuznetsov, Y.A.: Elements of applied bifurcation theory. 3rd edn. Springer-Verlag, New York (2004)

[27] Kuznetsov, Y.A., Muratori, S., Rinaldi, S.: Bifurcation and chaos in a periodic predator-prey model. Int J Bifurcat Chaos **2**, 117–128 (1993)

[28] Lavine, J.S., King, A.A., Bjrnstad, O.N.: Natural immune boosting in pertussis dynamics and the potential for long-term vaccine failure. Proc. Natl. Acad. Sci. U.S.A. **108**(17), 7259–7264 (2011). DOI 10.1073/pnas.1014394108. URL `http://dx.doi.org/10.1073/pnas.1014394108`

[29] Lipsitch, M., Viboud, C.: Influenza seasonality: lifting the fog. Proc. Natl. Acad. Sci. U.S.A. **106**(10), 3645–3646 (2009). DOI 10.1073/pnas.0900933106. URL `http://dx.doi.org/10.1073/pnas.0900933106`

[30] Pikovski, A., Rosenblum, M., Kurths, J.: Synchronization: A Universal Concept in Nonlinear Sciences. 1st edn. Cambridge University Press, New York (2003)

[31] Rinaldi, S., Muratori, S.: Conditioned chaos in seasonally perturbed predator-prey models. Ecol. Model. **69**(1-2), 79–97 (1993)

[32] Rinaldi, S., Muratori, S., Kuznetsov, Y.A.: Multiple attractors, catastrophes and chaos in seasonally perturbed predator-prey communities. B Math Biol **55**(1), 15–35 (1993)

[33] Schaffer, W., Pederson, B., Moore, B., Skarpaas, O., King, A., Bronnikova, T.: Sub-harmonic resonance and multi-annual oscillations in northern mammals: A non-linear dynamical systems perspective. Chaos Soliton Fract **12**(2), 251–264 (2001)

[34] Scheffer, M., Rinaldi, S., Kuznetsov, Y., Van Nes, E.: Seasonal dynamics of daphnia and algae explained as a periodically forced predator-prey system. Oikos **80**(3), 519–532 (1997)

[35] Tanaka, G., Aihara, K.: Effects of seasonal variation patterns on recurrent outbreaks in epidemic models. J. Theor. Biol. **317**, 87–95 (2013)

[36] Taylor, R.A., Sherratt, J.A., White, A.: Seasonal forcing and multi-year cycles in interacting populations: lessons from a predator-prey model. J. Math. Biol. pp. 1–24 (2012). DOI 10.1007/s00285-012-0612-z. URL `http://dx.doi.org/10.1007/s00285-012-0612-z`

[37] Upadhyay, R., Iyengar, S.: Effect of seasonality on the dynamics of 2 and 3 species prey-predator systems. Nonlinear Anal-Real **6**(3), 509–530 (2005)

[38] Vanlier, J., Tiemann, C.A., Hilbers, P.A., van Riel, N.A.: An integrated strategy for prediction uncertainty analysis. Bioinformatics **28**(8), 1130–1135 (2012). DOI 10.1093/bioinformatics/bts088. URL `http://dx.doi.org/10.1093/bioinformatics/bts088`